ACS APPLIED MATERIALS & INTERFACES

Research Article

www.acsami.org

Structure and Reactivity of Alucone-Coated Films on Si and Li_xSi_y Surfaces

Yuguang Ma,[†] Julibeth M. Martinez de la Hoz,[†,‡] Ivette Angarita,[†] Jose M. Berrio-Sanchez,[†] Laura Benitez,[†,§] Jorge M. Seminario,[†,‡,§] Seoung-Bum Son,[∥] Se-Hee Lee,[⊥] Steven M. George,[⊥] Chunmei Ban,[∥] and Perla B. Balbuena*[,†,‡]

[†]Department of Chemical Engineering, [‡]Department of Materials Science and Engineering, and [§]Department of Electrical Engineering, Texas A&M University, College Station, Texas 77843, United States

[∥]National Renewable Energy Laboratory, 1617 Cole Boulevard, Golden, Colorado 80401, United States

[⊥]University of Colorado at Boulder, Boulder, Colorado 80309, United States

Supporting Information

ABSTRACT: Coating silicon particles with a suitable thin film has appeared as a possible solution to accommodate the swelling of silicon upon lithiation and its posterior cracking and pulverization during cycling of Li-ion batteries. In particular, aluminum alkoxide (alucone) films have been recently deposited over Si anodes, and the lithiation and electrochemical behavior of the system have been characterized. However, some questions remain regarding the lithium molecular migration mechanisms through the film and the electronic properties of the alucone film. Here we use density functional theory, ab initio molecular dynamics simulations, and Green's function theory to examine the film formation, lithiation, and reactivity in contact with an electrolyte solution. It is found that the film is composed of Al−O complexes with 3-O or 4-O coordination. During lithiation, Li atoms bind very strongly to the O atoms in the most energetically favorable sites. After the film is irreversibly saturated with Li atoms, it becomes electronically conductive. The ethylene carbonate molecules in liquid phase are found to be reduced at the surface of the Li-saturated alucone film following similar electron transfer mechanisms as found previously for lithiated silicon anodes. The theoretical results are in agreement with those from morphology and electrochemical analyses.

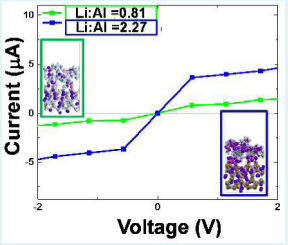

KEYWORDS: *density functional theory, alucone coating, silicon anodes, lithium-ion batteries, structural changes from lithiation, solid-electrolyte-interphase*

INTRODUCTION

The most common anode material for lithium-ion batteries is graphite due to its relatively low cost and relatively long cycle life. However, graphite anodes have some issues related to their low energy density (LiC_6, 372 mAh g^{-1}, 804 Ah/L) and safety (low operation voltage), which need to be improved. Silicon, an alternative Li-ion anode material, stores 10 times more lithium ($Li_{22}Si_5$, 4200 mAh g^{-1}; $Li_{15}Si_4$, 3579 mAh g^{-1}, 8343 Ah L^{-1}) than the current commercial graphite anode and moderate operation potential versus lithium.[1,2] Numerous studies have investigated the intrinsic properties of silicon upon lithiation and delithiation[3−9] accompanied by large volumetric changes up to ∼300%.[10] This impedes the practical application of silicon as anode materials, as this may lead to cracking and pulverization of particles, making Si anodes lack sufficient stability to sustain hundreds of charge/discharge cycles in Li-ion batteries.[4,5] Moreover, during the electrochemical reactions, a solid electrolyte interphase (SEI) layer is formed on the anode surface, leading to undesirable interfacial interactions that inevitably consume lithium.[11] The process results in a series of side effects, including large initial irreversible capacity, low specific capacity, high impedance, and incomplete lithiation.[12,13] However, the SEI layer may effectively limit the volume expansion of silicon upon lithiation and thus enhance the cycle stability.[14]

An effective method to improve cycling performance of lithium-ion batteries is surface modification, which can enhance the ionic and electric conductivity, accommodate volumetric changes, prevent particle agglomeration, and modify surface conditions favoring a robust interface.[5,15−18] In recent years, atomic layer deposition (ALD) and molecular layer deposition (MLD) have been developed for boosting the stability of Li-ion electrodes.[19−22] By using these methods, continuous and conformal films deposit on silicon anodes, forming a thin layer of coating that can effectively protect electrodes. For example, in comparison to the fast decay observed in a bare silicon anode, MLD alucone-coated silicon anodes show sustainable cycling performance with a high Coulombic efficiency above 99.9%.[22] More attractively, the approach allows optimization of the mechanical properties without sacrificing rate capability of high-energy electrodes.

In this study, we focus on a hybrid organic−inorganic film fabricated using sequential, self-limited reactions between

Received: March 3, 2015
Accepted: May 19, 2015
Published: May 19, 2015

DOI: 10.1021/acsami.5b01917
ACS Appl. Mater. Interfaces 2015, 7, 11948−11955

trimethylaluminum (TMA) and glycerol. The aluminum alkoxide (alucone) coating possesses a 3D network structure $[-Al_n(-OCH_2-CHO-CH_2O-)_m$ $(n{:}m = 1)]$ on the surface of silicon nanoparticles. Interestingly, the alucone-coated anodes show some distinct electrochemical behaviors.[22] The structural and chemical evolution of MLD alucone-coated Si nanoparticles has been examined by using in situ transmission electron microscopy (TEM).[11] The results revealed that the native oxide layer on the Si particles has negative effects on electrochemical performance. The alucone MLD coating procedures, however, almost fully removed the native oxide layer. The coating layer exhibits excellent flexibility, surviving in the drastic volumetric expansion/shrinkage of the silicon nanoparticle upon lithiation and delithiation. In addition, conductivity measurements also indicate a substantial improvement of electrical conductivity of the lithiated alucone coating.[11]

MLD coating has shown great potential for remarkable improvement of Li-ion battery performance. Although experimental investigations[11,22,23] have revealed some important details about MLD-deposited films, there are still several questions regarding the structural and protection mechanisms of the films that remain unresolved. Molecular simulations and theoretical calculations may play a critical role to explore these issues; in particular, when combined with state-of-the-art experimental technologies, understanding molecular level mechanisms becomes possible. Here we use density functional theory (DFT), ab initio molecular dynamics (AIMD), and DFT-Green's function analysis to examine the possible formation reactions and structure of the alucone film, lithiation mechanisms, electronic conductivity, and reactivity of the film in contact with the electrolyte as a function of its degree of lithiation. We discuss the results comparing them with experimental results from morphology and electrochemical analyses toward better understanding the impact of this alucone coating on the cycling behavior and interfacial chemistry of Si anodes.

METHODOLOGY

Computational Details. Periodic DFT calculations were performed to evaluate the film formation reactions using the Vienna ab initio simulation package (VASP 5.3),[24−27] which solves self-consistently the Kohn−Sham equations. The exchange-correlation functional was described within the generalized gradient approximation (GGA) proposed by Perdew, Burke, and Ernzerhof (PBE).[28] For improving the computational efficiency, the projector augmented wave (PAW) pseudopotentials were applied to the core electrons,[29,30] while the valence electrons were described by plane wave basis sets with a cutoff energy of 400 eV. For surface adsorption calculations, the Brillouin zone was sampled with a $2 \times 2 \times 1$ Γ centered k-mesh in the reciprocal space. The Gaussian smearing method was employed to determine electron occupancies with a smearing width of 0.05 eV. The convergence criterion of structure relaxation was set to 0.05 eV/Å.

AIMD simulations were conducted on the optimized Si(001) surface in contact with a layer of alucone film, using the NVT ensemble. The time step was set to 1 fs, and the Nose thermostat was employed to control the temperature oscillations during the simulation with a Nose-mass parameter of 0.5, which gives a frequency of oscillation corresponding to 176 time steps. Brillouin zone Γ point sampling was applied in this case with a plane wave energy cutoff of 400 eV. In each simulation, ethylene carbonate (EC) molecules and Li atoms were placed in certain positions in the film to determine Li^+ diffusion. AIMD simulations were also employed on DFT optimized Li_xSi_y surfaces in contact with a layer of alucone film, interacting with EC molecules. Lithium atoms were placed in the most energetically favorable positions (as determined from the DFT optimizations) in the alucone film. The NVT ensemble at 450 K was used in order to simulate liquid EC in contact with the film-covered Li_xSi_y surface. The same setting was used to examine the reactivity of the coated surface.

Cluster calculations were carried out to evaluate details of the film structure and its lithiation using the hybrid B3PW91 functional which is composed of Becke's three parameter gradient-corrected exchange functional[31] and the Perdew−Wang 91 correlation functional.[32] The hybrid functional, B3PW91, has shown its reliability for the electronic structure calculations in lithium-ion batteries.[33−35] Both the geometry optimization and the single-point calculations were carried out using a 6-311++G(d,p) basis set. Second derivatives were computed for verifying local minima, determining transition states, and estimating zero-point energy (ZPE) and thermal corrections.

The Si(100) 2×1 surface was simulated by a slab model with a 5×5 unit cell, consisting of 5 Si layers and 5 nm vacuum. The vacuum layer is partially filled by alucone polymers for investigating the properties of the film. The vacuum layer is reduced to 2−4 nm under such conditions. The top 3 layers of the Si(001) were allowed to relax to their lowest energy configuration, while the bottom 2 layers were fixed to the bulk positions keeping their optimized lattice constants. For both periodic and cluster calculations, the corresponding adsorption energy, E_{ads}, is defined by the following equation: $E_{ads} = E_{sub/ads} - E_{sub} - E_{adsorbate}$, in which $E_{sub/ads}$ is the total energy of the optimized substrate−adsorbate structures, E_{sub} is the energy of the substrate, and the $E_{adsorbate}$ is the energy of adsorbate, both in free states.

The electronic conductivity of the film was evaluated utilizing the DFT-Green's function method described in our previous work.[36] Briefly, a composite interfacial system is built that is composed by a model Li_xSi_y electrode covered by the lithiated alucone layer. An applied potential is imposed between two gold nanoelectrodes triggering the leakage current that would occur during battery charge (Figure 1).

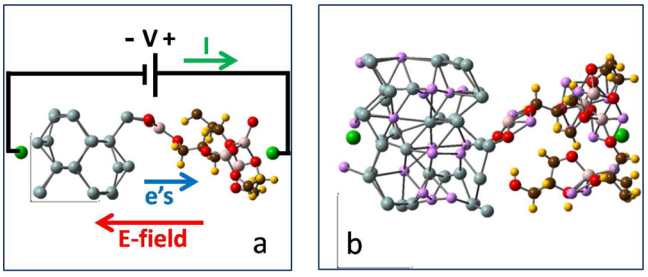

Figure 1. Model used for evaluations of electron transfer through the film. (a) The schematic represents a piece of the coated Li_xSi_y electrode. Both ends of the composite interface are connected to nanogold contacts (green spheres), which are used to apply an external applied potential (V). Such applied potential induces an electric field (E) at the interface and is the driving force for the leakage current that would occur during charging of the battery. When the negative of the source V is applied to the Li_xSi_y side, electrons move from the Li_xSi_y to the film, opposite to the conventional current (I) of positive carriers. (b) Actual model used for $Li_{18}Si_{36}$-$C_{14}Li_{11}Al_5O_{15}H_{26}$. Color code: gray, Si; red, O; yellow, H; pink, Al; brown, C; purple, Li.

The current−applied potential (I−V) curves are calculated using the transmission function $T(E, V)$ using the Landauer equation[37−41]

$$I \approx \frac{2e}{h} \int_{E_f+V_1}^{E_f+V_2} T(E, V)\, dE \qquad (1)$$

Here, e is the charge of the electron, h is the Planck constant, $T(E, V)$ is the transmission function, E is the energy, and E_f is the Fermi level of the molecular junction.

The transmission function is calculated using the following expression (see for instance[42])

DOI: 10.1021/acsami.5b01917
ACS Appl. Mater. Interfaces 2015, 7, 11948−11955

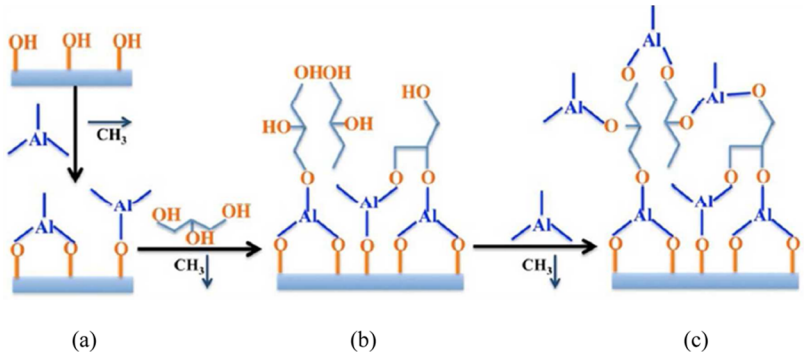

Figure 2. Schematic diagram showing the alucone layer formation process on Si particle surfaces covered with native oxide. a, b, and c indicate the successive reaction stages. Reprinted with permission from ref 11. Copyright 2014 American Chemical Society.

$$T(E, V) = Tr(T_1(E, V)G_M(E, V)T_2(E, V)G_M^+(E, V) \quad (2)$$

where $T_k = i(\sum_k^- - \sum_k^+)$ $(k = 1, 2)$ is the coupling between the electrodes and the molecule, G_M is the retarded Green function, and G_M^+ is its adjoint. G_M is obtained using

$$G_M(E, V) = [ES_{MM}(E, V) - H_{MM}(E, V) - \sum_1 (E, V) - \sum_2 (E, V)]^{-1} \quad (3)$$

$\sum_k(E, V) = H_{Mk}g_k(E)H_{kM}$ for $k = 1, 2$ is the self-energy from the contacts. S_{MM} and H_{MM} are the overlap and Hamiltonian submatrices corresponding to the composite interfacial system; they are obtained from the global Schrödinger equation

$$H(V)\varphi(V) = \varepsilon(V)S(V)\varphi(V) \quad (4)$$

once the wave function $\varphi(V)$ is obtained in a self-consistent manner.

Experimental Details. Silicon nanoparticles (50 nm) were purchased from Alfa Aesar and used to make the nanocomposite electrode with acetylene black (AB), and PVDF (polyvinylidene fluoride, binder) (60:20:20 weight ratio). Alucone coating was directly grown on the Si electrode by using MLD reaction of trimethylaluminum and glycerol. The fabrication process of the electrode and MLD coating were reported in previous papers.[22] HAADF (high angle annular dark field)-STEM (scanning transmission electron microscope) was performed with an FEI Tecnai F20 equipped with STEM operated at 200 keV.[22] Coin cells were used to test the electrochemical properties of the alucone film, which was deposited on the stainless steel with a designed thickness. The coin cells were assembled in an Ar-filled glovebox using the alucone film as the working electrodes and lithium metal foil as the counter electrode. The electrolyte was 1 M LiPF6 dissolved in a 1:1 (volume ratio) mixture of ethylene carbonate (EC) and diethyl carbonate (DEC); the separator was a glass microfiber disk (WhatmanTM GF/F), and the shell was a stainless steel CR2032 coin cell. All of electrochemical cycling was carried out using Biologic VMP3.

RESULTS AND DISCUSSION

Film Formation and Structure. Experimental evidence has indicated that the alucone MLD coating removed the native oxide, leading to a covalently bonded and fully nucleated alucone layer (2−5 nm) on Si particles.[22,11] As the first step of the process, trimethyl aluminum, a metal precursor for the coating process, reacts with the surface silanol groups of the native oxides. We study the two corresponding reactions illustrated in Figure 2a, where the methyl group is abbreviated as Me:

$$AlMe_3 + HO\text{-}Si(001) \rightarrow AlMe_2{-}O{-}Si(001) + CH_4 \quad (5)$$

$$AlMe_3 + (HO)_2\text{-}Si(001) \rightarrow AlMe{-}O_2{-}Si(001) + 2CH_4 \quad (6)$$

The calculated reaction energies are −1.86 eV for reaction 5 and −3.00 eV for reaction 6, indicative of both reactions being thermodynamically favorable. This confirms that the alucone coating is covalently bound to the Si surface, which ensures mechanical integrity in the coated electrode. The adsorbed CH_3−Al group can react with glycols, such as ethylene glycol and glycerol, followed by the further glycol-TMA reactions, and finally formation of amorphous 3D-network structures with chemical composition of $-Al_n(-OCH_2-CHO-CH_2O-)_m$ $(n{:}m = 1)$.[11] These reaction steps are also exothermic: For instance, the following reactions (products shown in Figure 2b) possess reaction energies of −1.20 eV for reaction 7 and −2.61 eV for reaction 8.

$$AlMe{-}O_2{-}Si(001) + \text{glycerol} \rightarrow HOCH_2CHOHCH_2O{-}Al{-}O_2{-}Si(001) + CH_4 \quad (7)$$

$$AlMe_2{-}O{-}Si(001) + 2\text{glycerol} \rightarrow (HOCH_2CHOHCH_2O)_2{-}Al{-}O{-}Si(001) + 2CH_4 \quad (8)$$

The overall coating process is accordingly energetically favorable. Further reactions with TMA determine film growth as shown in Figure 2c. Moreover, our DFT calculations show that the partially oxidized Si(001) surface is distorted in the coating process. The Si atoms bonding with oxygen are typically stretched out of the surface ∼0.2 Å. The bond length of newly formed Al−O is around 1.7 Å. For the adsorbed Me_2Al− and MeAl− groups, the bond lengths of Al−C show no obvious change compared to that in TMA, as shown in Figure 3.

The experimentally measured density of the thin film is ∼1.6−1.7 g cm^{-3} while the film was grown at 140−150 °C, respectively.[43] Considering the composition of the film, each single unit of the polymer, $-C_3H_5O_3Al-$, occupies a volume of ∼120 $Å^3$. Therefore, the 3D network must be packed very tightly, as the minimum volume of single unit packing is ∼103 $Å^3$. On the basis of this information, we infer that many cross-links and branch chains must be formed in the structure, because such connection modes allow utilizing the space maximally. This is in good agreement with experimental results, in which a dense and conformal coating of alucone adhered to the nano-Si particle is observed using high-resolution HAADF-STEM as shown in Figure 4. Recent results from in situ TEM

DOI: 10.1021/acsami.5b01917
ACS Appl. Mater. Interfaces 2015, 7, 11948−11955

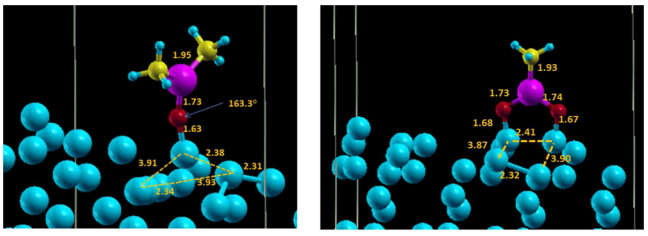

(a) (b)

Figure 3. Optimized geometry of the Me_2Al- (a) and $MeAl-$ (b) adsorption on Si−Li oxide surface. The light blue, red, purple, and yellow spheres represent Si, O, Al, and C atoms, respectively. The marked distances are in Å.

also show the uniform coverage of the alucone film on the Si particles.[11]

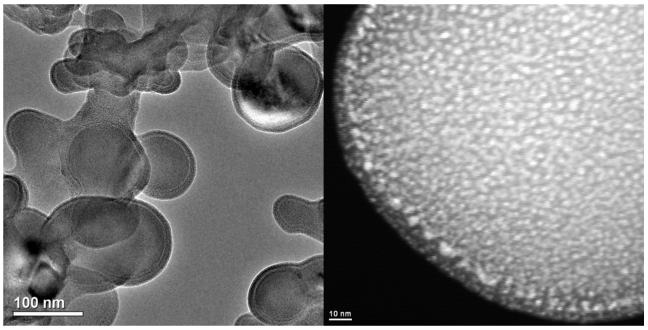

Figure 4. High-resolution HAADF-STEM images of the alucone-coated Si particles in different magnifications, confirming that a thin (∼5 nm), dense, and conformal coating of alucone adhered to the nano-Si particle.

Since the thickness of the polymer film could reach up to several nanometers (3−5 nm) on the Si electrode surface, we built a slab model to examine the adsorption and diffusion properties. The periodic model is composed of 5 layers of Si, ∼3 nm alucone, and ∼2 nm vacuum. The alucone polymer has multi-cross-links connected by Al−O bonds, as illustrated in Figure 3a. The density of the constructed polymer is ∼1.5 g cm^{-3}, comparable to the experimental value. In the initial configuration, each Al atom is bonded with 3 oxygen atoms (Figure 5a). After DFT optimization, three bonding modes of Al are identified in the film: **1**, each Al atom bonded with 4 O atoms in a slighted distorted tetrahedron configuration; **2**, each Al atom connected 3 O atoms, forming a pyramid configuration; and **3**, each Al atom coordinated with 3 atoms, but basically in a planar configuration (Figure 5b). For **2** and **3**, the bond length of Al−O is usually around 1.67−1.73 Å; while for **1**, typically three Al−O bonds are in the range 1.70−1.80 Å, and the fourth one is a little longer, ∼1.90 Å. Short AIMD simulations of the optimized structure at 400 K show that the configurations are generally sustained.

The periodic DFT results suggested that 4-O coordinated Al complexes could be formed in the film if nearby O atoms are available. An interesting question follows: Which configuration is more stable, 3- or 4-O coordinated Al complexes? We used a cluster model to compare the stability of the Al-complexes. As shown in Figure 6, **A** is built as a 3-O coordinated complex with 3-O and an Al atom, while **B** and **C** are 4-O coordinated complexes in which **C** contains CH_3CH_2OH as the fourth ligand. The optimized structures have a similar Al−O bond

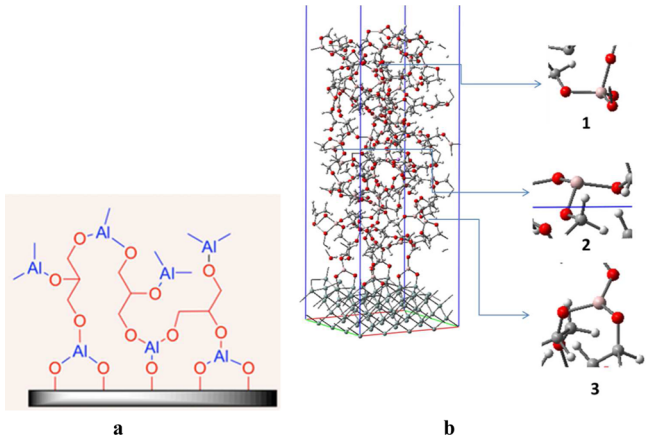

Figure 5. (a) Plausible structure of alucone coating film; (b) DFT optimized film structure based on the slab model. **1**, **2**, and **3** are coordination modes of Al to O in the film (see text). The light blue, pink, red, gray, and white spheres represent respectively Si, Al, O, C, and H atoms.

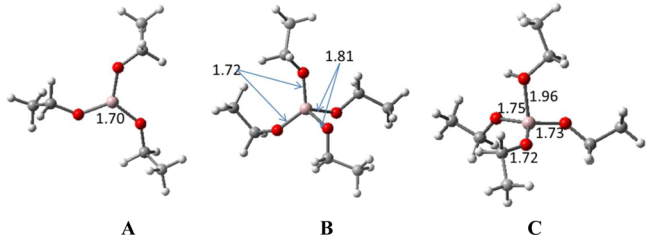

Figure 6. Cluster models of 3- and 4-coordinated Al complexes: **A**, 3-O coordination; **B**, 4-O coordination; **C**, 4-O coordination with a terminal OH group. The listed distances are in Å. Color code as in Figure 4

length compared to those in the slab model. **B** and **C** are produced by the following addition reactions: **A** + CH_3CHO- → **B** and **A** + CH_3CHOH → **C**. The corresponding reaction energies are −1.06 and −0.91 eV, respectively. Therefore, introducing a fourth ligand into the 3-coordinated Al complex is energetically feasible, and accordingly configuration **1** (Figure 5b) is stable in the film structure.

Film Lithiation. It is of importance to understand the possible lithiation in the film, as it may considerably influence the electrochemistry of the Si anodes. On the other hand, the film structure may be modified in the process of lithiation. The structural change could induce some effects on the stability of the film. As a first step, Figure 7 displays the use of the simple cluster models, **A**, **B**, and **C** (Figure 6), to investigate lithiation in the alucone film.

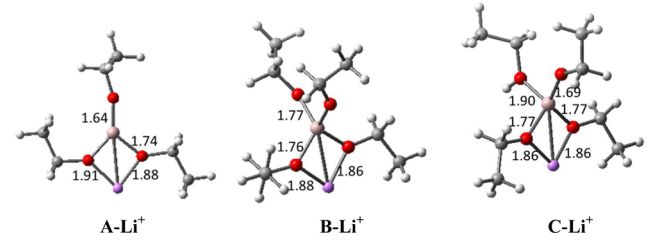

Figure 7. Li^+ binding on cluster model **A**, **B**, and **C**. The listed distances are in Å. Li^+ ions are denoted as purple spheres. The color code for the other atoms is as in Figure 4

DOI: 10.1021/acsami.5b01917
ACS Appl. Mater. Interfaces 2015, 7, 11948−11955

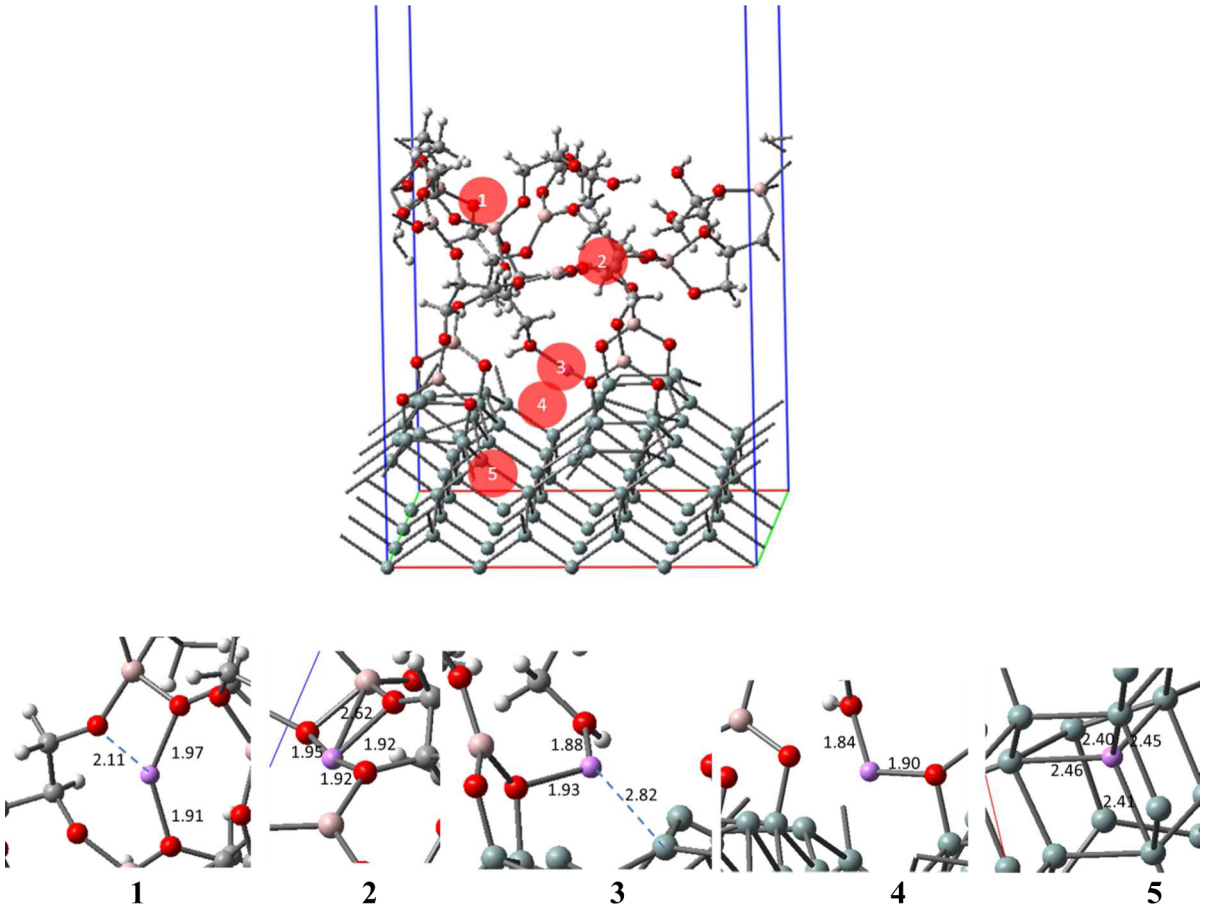

Figure 8. Li binding sites (**1**–**5**) in the slab model. For each binding site, the nearby optimized geometry is depicted. The listed distances are in Å.

For all the configurations, Li^+ is bound with 2 oxygen atoms. The bond length of Li–O is around 1.9 Å. Our calculations indicate that all the configurations can bind Li^+. The corresponding values of binding energy are −2.63 eV for **A**, −3.15 eV for **B**, and −3.30 eV for **C**, suggesting very strong Li bindings on all the complexes. The result implies that Li ions may reside in the film, thus leading to some irreversible capacity. Notably, Li^+ binding is stronger in the 4-O coordination complex. We may thus deduce that the lithiation may first take place in those sites.

We further examine the Li^+ binding in different positions of the film and Si surface. For this purpose, a slab model containing 5-layer Si(001) and film of 1 nm thickness is constructed. Li^+ is located in 5 different initial positions, ranging from the film outer surface to the inner layer of Si(001), as depicted in Figure 8. For each initial configuration, stable binding sites are obtained after DFT geometry optimization. As Li^+ carries positive charge and the O atoms are the negative charge centers in the film, it is straightforward that the electrostatic interactions of Li^+ and O provide the primary contribution for the binding. In positions **1** and **2** (Figure 8), there are 3 O atoms involved in the Li^+ binding; the Li–O distance varies from 1.9 to 2.1 Å. Configurations **3** and **4** are closer to the Si(001) surface, and each one only has 2 neighboring O around Li^+. Notably, although locations **3** and **4** (Figure 8) are located near the Si surface initially, no strong Si–Li interaction was found: The shortest Si–Li distance is 2.82 Å for the optimized structures. These results reveal that the Li–O interactions are predominant in the film, and even on the film/Si interface. In **5**, Li^+ is positioned in the Si subsurface, and it binds with 4 neighboring Si atoms. The calculated binding energies are listed in Table 1. Here we use the binding energy of **1** as a reference, and the value is set to 0. According to the calculated binding energies, the binding strength orders as **1** > **2** > **3** > **4** > **5**. Compound **1** shows the strongest Li^+ binding, whereas the weakest binding strength is found in **5**. Interestingly, the order is consistent with the positions of Li^+ in the slab model: Li^+ binding on the upper surface of the film is the strongest one. The strength is gradually reduced with Li^+ moving inside the film, reaching on the film/Si interface and entering into the Si bulk. This analysis suggests that the lithiation starts at the alucone coating film, in particular, on the surface of the 3D network. Furthermore, considering the strong O–Li interactions, the Li^+ release process from the film is unlikely to happen, and the film lithiation involving saturation of the favorable sites discussed in Figure 7 may be considered as

Table 1. Calculated Li^+ Binding Energies at Different Sites in the Film[a]

configuration	distance of Li^+ to Si(001) surface (Å)	binding energy (eV)
1	7.95	0
2	4.02	2.13
3	1.73	2.73
4	1.40	2.87
5	−2.66	4.15

[a]The binding energy of **1** is set to 0 as a reference. The configurations are shown in Figure 7.

DOI: 10.1021/acsami.5b01917
ACS Appl. Mater. Interfaces 2015, 7, 11948–11955

irreversible. In order to confirm the irreversible storage of lithium ion in the alucone film, the 1.2 nm MLD alucone film was coated on stainless steel and electrochemically cycled against Li metal. It shows that the MLD film has an irreversible capacity loss of 48% (Supporting Information, Figure S1), which agrees well with the calculated results. Additionally, the increase in thickness of this alucone coating layer after lithiation was observed under in situ TEM characterization.[11] It is expected that volume expansion occurs to accommodate lithium insertion in this super dense film. Therefore, lithiation starting from the alucone layer expands the film to further accommodate the large volume expansion of Si particles.

We also examined atomic charge evolution of the film during lithiation. Figure S2 (Supporting Information) shows that there is a very slight reduction in the average charge of the Al atoms (from an average of +2.39 at Li:Al ratio = 0.09 to an average of +2.22 at 0.90 Li:Al ratio) and a corresponding slight increase in the average charge on O atoms (from −1.37 to −1.42, respectively), whereas the charges on Li and C atoms remain constant. Thus, the electrons contributed by the new Li atoms incorporated into the film are distributed among the O and Al atoms. Further information about changes in the electronic distribution during lithiation is obtained from electron density maps. Figure S3 (Supporting Information) reveals how the electron density is accumulated surrounding the O atoms while electron-depleted regions surround the Al and Li atoms. Since the film possesses a relatively high degree of porosity, Li-ion transport should be facilitated by the presence of the electron-rich regions that increase with the Li concentration (Supporting Information Figure S3). Recent work[44] has suggested that Li ions may diffuse via a knock-off mechanism in porous crystalline structures such as Li_2CO_3 in order to maintain high O coordination, and this mechanism would be preferred to direct hopping through empty spaces in the lattice. Our analysis of binding geometries and energies (Figure 8 and Table 1) along with the existence of electron-rich regions (Supporting Information Figure S3) that may facilitate relatively fast Li transport suggests that the most favorable knock-off mechanism may be also favorable in the alucone film. It is also interesting to compare the alucone film lithiation with that in other coatings such as Al_2O_3 recently discussed by Kim and Qi.[45] These authors suggest a conversion of alumina to $LiAlO_2$ as it lithiates, which is accompanied by a substantial decrease in the barrier for Li diffusion. A similar behavior may be expected in alucone on the basis of our simulated results.

Film Reactivity. For the alucone-film-coated lithiated Si particles, Li distribution in the surface of Si particles should be affected due to the strong Li binding in the film. We carried out AIMD simulations to examine the possible Li migration from the lithiated Si to the film. The slab model contains 5 layers of $Li_{11}Si_{12}(001)$ and 1 nm layer of alucone film, and the simulation lasts ~2 ps at 450 K. Some Li atoms were found to migrate from the lithiated surface to the film (not shown). This further verifies that the film is preferred for lithiation in comparison to the Si nanoparticles.

The strong Li binding in the film suggests that reduction reactions may take place on the surface covered by the alucone film. To test the possibility, we examined the reactivity of electrolytes on the film surface. In the study, ethylene carbonate (EC) is used as the electrolyte. Two slab models, respectively, including 5 layers of Si(001) and $Li_{11}Si_{12}(001)$, covered by a 1 nm thickness film are employed (Figure 9).

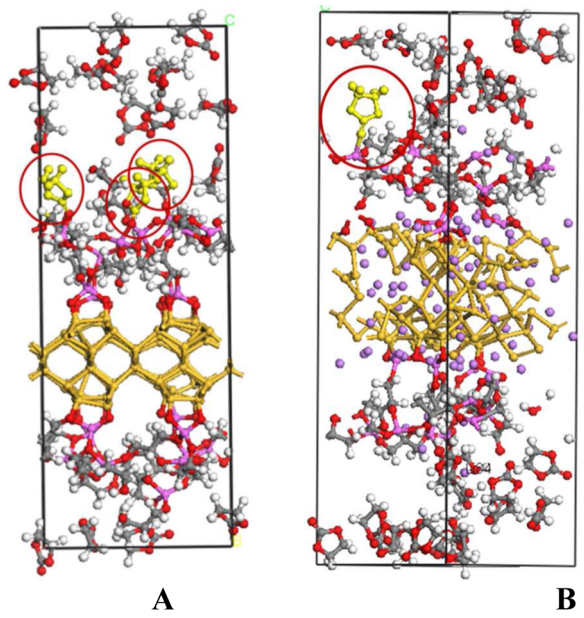

Figure 9. AIMD simulations illustrating EC adsorption on an unlithiated alucone film surface. **A** and **B** include 5 layers of Si(001) and $Li_{11}Si_{12}(001)$, respectively. The EC adsorption sites are circled by red lines. No EC reduction is observed in this case.

The AIMD simulations show that EC molecules are strongly adsorbed on the film surface in both models where the EC carbonyl oxygen bonds with Al atoms from the film (Figure 9). In **B**, some of the Li atoms diffuse from the electrode into the film. Although EC is bound onto Al atoms, no decomposition reaction is captured during the simulation period (4.5 ps), most likely due to a lack of conductive routes for electrons in the low-lithiated film.

However, our experimental results indicate the lithiated alucone film is both electronically and ionically conductive.[11] To further investigate this point, we evaluate two additional models: in the first the film is completely saturated with Li atoms located in all possible most favorable lithiation sites as discussed in relation to Figure 7. In the second model the film is supersaturated; that is, the Li concentration goes beyond saturation of the most favorable sites. These additional Li atoms were added in random locations to the film. The binding energies of these sequential Li additions were computed (Supporting Information, Figures S4 and S5). It is observed that the slope of binding energy versus the amount of Li in the film changes drastically beyond the saturation point with the binding becoming much less favorable. Thus, further Li atoms passing through the film beyond its saturation point will not be strongly retained; instead, their diffusion will be facilitated as required during charge or discharge of the battery. The calculated results agree well with the experimental data. The fast lithiation process has been confirmed for the coated Si anode, which enables the coated Si anode to cycle at high cycling rates.[22]

To assess the film's electronic conductivity, we used the procedure described in Figure 1 applied to the $Li_{18}Si_{36}$ model of the anode covered by two different films: a "saturated" film represented by $C_{14}\mathbf{Li_5}Al_5O_{15}H_{26}$ where all the 5 Al−O_x groups are coordinated with Li, and a "supersaturated" film of composition $C_{14}\mathbf{Li_{11}}Al_5O_{15}H_{26}$ where there are 6 extra Li atoms added to random locations in the film. The results are shown in Figure 10.

DOI: 10.1021/acsami.5b01917
ACS Appl. Mater. Interfaces 2015, 7, 11948−11955

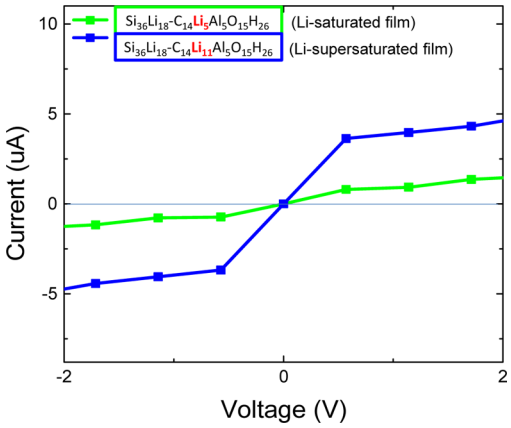

Figure 10. Electron current determined for various values of applied voltage for the two model systems. A clear enhancement of the electron conductivity is found in the supersaturated film.

In agreement with the experimental results, the calculated electronic conductivity shows that the lithiated film is able to conduct electrons, and such ability increases as the lithiation goes beyond saturation of the film.

The ability of the film to conduct electrons may induce the reduction of the electrolyte species and form a passivation layer on the surface of the lithiated alucone film, as determined by new AIMD simulations. We found fast EC reduction on both the saturated and supersaturated films. For the saturated and supersaturated films, sequential two electron transfer happens in two steps: first the EC molecule receives an electron from the surface and becomes an open EC^{-} radical, which after a second electron transfer becomes CO_3^{2-} and C_2H_4. In another surface, EC is reduced to open EC^{2-} receiving 2 electrons simultaneously from the surface. The open EC^{2-} radical anion is further reduced to CO^{-2} and $O(C_2H_4)O^{2-}$, another radical anion. These are just examples of the multiple reactions that can be observed at this high lithiation degree, which are similar to the initial reactions leading to nucleation of SEI products on the coated electrode found in other highly lithiated surfaces.[46−48] However, with the involvement of the alucone film, the reduction of EC may contribute to a new-type of SEI. Investigations are ongoing to understand the effect of coating (especially the Al-Ox groups) on the chemistry of the SEI.

CONCLUSIONS

DFT calculations have been applied to study the growth mechanism and structure of the MLD alucone coating for Si particles. The results reveal that a compact alucone film is formed by thermodynamically favorable reactions between trimethyl aluminum and the silanol groups of the surface and posterior reaction with glycerol. A dense and conformal coating is enabled by numerous cross-links connected by Al−O bonds. First-principles analyses of alucone-coated silicon particles illustrate the molecular mechanisms of lithium irreversible binding in the alucone coating. Aluminum is found in three coordination modes, and these functional structures are the basis for Li binding with values ranging −2.63 to −3.30 eV. Considering these strong Li−O interactions, the lithiation of the film involving these most favorable sites may be considered irreversible. In agreement with the experimental results, the irreversible lithiation process modifies the electronic and ionic transport properties and consequently the reactivity of the alucone coating. Once the lithium atoms occupy all the favorable sites, the film becomes electronically conductive, and ethylene carbonate molecules easily decompose on its surface following similar electron transfer mechanisms as detected previously on lithiated silicon anodes. The current analysis explains how a passivation SEI layer may be formed over the surface of the lithiated film once most of the favorable Li binding sites are occupied by irreversibly adsorbed Li.

ASSOCIATED CONTENT

Supporting Information

Figure S1 depicting the galvanostatic cycling curve of a 1.2 nm alucone film. Figure S2 showing the average atomic charges inside the film during lithiation. Figure S3 depicting electron density maps on a plane located inside the alucone film and parallel to the anode surface. Figures S4 and S5 showing the binding energies of Li atoms to the alucone film covering a pure Si and a LiSi surface, respectively. The Supporting Information is available free of charge on the ACS Publications website at DOI: 10.1021/acsami.5b01917.

AUTHOR INFORMATION

Corresponding Author

*E-mail: balbuena@tamu.edu.

Notes

The authors declare no competing financial interest.

ACKNOWLEDGMENTS

This work was supported by the Assistant Secretary for Energy Efficiency and Renewable Energy, Office of Vehicle Technologies of the U.S. Department of Energy under Contract No. DE-AC02-05CH11231, Subcontract No. 7060634 under the Advanced Battery Materials Research (BMR) Program. Computational resources from the Texas A&M Supercomputing Center, Brazos Supercomputing Cluster at Texas A&M University, and Texas Advanced Computing Center at UT Austin are gratefully acknowledged.

REFERENCES

(1) Zhang, W. J. A Review of the Electrochemical Performance of Alloy Anodes for Lithium-Ion Batteries. *J. Power Sources* **2011**, *196*, 13−24.

(2) Chan, C. K.; Peng, H. L.; Liu, G.; McIlwrath, K.; Zhang, X. F.; Huggins, R. A.; Cui, Y. High-Performance Lithium Battery Anodes using Silicon Nanowires. *Nat. Nanotechnol.* **2008**, *3*, 31−35.

(3) Liu, X. H.; Zhong, L.; Huang, S.; Mao, S. X.; Zhu, T.; Huang, J. Y. Size-Dependent Fracture of Silicon Nanoparticles During Lithiation. *ACS Nano* **2012**, *6*, 1522−1531.

(4) Kasavajjula, U.; Wang, C. S.; Appleby, A. J. Nano- and Bulk-Silicon-Based Insertion Anodes for Lithium-Ion Secondary Cells. *J. Power Sources* **2007**, *163*, 1003−1039.

(5) Zhang, L. Q.; Liu, X. H.; Liu, Y.; Huang, S.; Zhu, T.; Gui, L. J.; Mao, S. X.; Ye, Z. Z.; Wang, C. M.; Sullivan, J. P.; Huang, J. Y. Controlling the Lithiation-Induced Strain and Charging Rate in Nanowire Electrodes by Coating. *ACS Nano* **2011**, *5*, 4800−4809.

(6) Xu, K. Nonaqueous Liquid Electrolytes for Lithium-Based Rechargeable Batteries. *Chem. Rev.* **2004**, *104*, 4303−4417.

(7) Philippe, B.; Dedryvere, R.; Allouche, J.; Lindgren, F.; Gorgoi, M.; Rensmo, H.; Gonbeau, D.; Edstrom, K. Nanosilicon Electrodes for Lithium-Ion Batteries: Interfacial Mechanisms Studied by Hard and Soft X-ray Photoelectron Spectroscopy. *Chem. Mater.* **2012**, *24*, 1107−1115.

(8) Arreaga-Salas, D. E.; Sra, A. K.; Roodenko, K.; Chabal, Y. J.; Hinkle, C. L. Progression of Solid Electrolyte Interphase Formation on Hydrogenated Amorphous Silicon Anodes for Lithium-Ion Batteries. *J. Phys. Chem. C* **2012**, *116*, 9072−9077.

DOI: 10.1021/acsami.5b01917
ACS Appl. Mater. Interfaces 2015, 7, 11948−11955

(9) McArthur, M. A.; Trussler, S.; Dahn, J. R. In Situ Investigations of SEI Layer Growth on Electrode Materials for Lithium-Ion Batteries Using Spectroscopic Ellipsometry. *J. Electrochem. Soc.* **2012**, *159*, A198−A207.
(10) Gu, M.; Xiao, X. C.; Liu, G.; Thevuthasan, S.; Baer, D. R.; Zhang, J. G.; Liu, J.; Browning, N. D.; Wang, C. M.: Mesoscale Origin of the Enhanced Cycling-Stability of the Si-Conductive Polymer Anode for Li-ion Batteries. *Sci. Rep.* **2014**, *4*.
(11) Yang, H.; M. P, D.; Gu, M.; Travis, J. J; George, S. M.; Lee, S.-H.; Genc, A.; Pullan, L.; Liu, J.; Mao, S. X.; Zhang, J.-G.; Ban, C.; Wang, C. In Situ Transmission Electron Microscopy Probing of Native Oxide and Artificial Layer on Silicon Nanoparticles for Lithium Ion Battery. *ACS Nano* **2014**, *8*, 11816−11823.
(12) Xun, S.; Song, X.; Wang, L.; Grass, M. E.; Liu, Z.; Battaglia, V. S.; Liu, G. The Effects of Native Oxide Surface Layer on the Electrochemical Performance of Si Nanoparticle-Based Electrodes. *J. Electrochem. Soc.* **2011**, *158*, A1260−A1266.
(13) Nagao, Y.; Sakaguchi, H.; Honda, H.; Fukunaga, T.; Esaka, T. Structural Analysis of Pure and Electrochemically Lithiated SiO using Neutron Elastic Scattering. *J. Electrochem. Soc.* **2004**, *151*, A1572−A1575.
(14) Wu, H.; Chan, G.; Choi, J. W.; Ryu, I.; Yao, Y.; McDowell, M. T.; Lee, S. W.; Jackson, A.; Yang, Y.; Hu, L. B.; Cui, Y. Stable Cycling of Double-Walled Silicon Nanotube Battery Anodes through Solid-Electrolyte Interphase Control. *Nat. Nanotechnol.* **2012**, *7*, 309−314.
(15) Wang, C.; Wu, H.; Chen, Z.; McDowell, M. T.; Cui, Y.; Bao, Z. A. Self-Healing Chemistry Enables the Stable Operation of Silicon Microparticle Anodes for High-Energy Lithium-Ion Batteries. *Nat. Chem.* **2013**, *5*, 1043−1049.
(16) Liu, Y.; Hudak, N. S.; Huber, D. L.; Limmer, S. J.; Sullivan, J. P.; Huang, J. Y. In Situ Transmission Electron Microscopy Observation of Pulverization of Aluminum Nanowires and Evolution of the Thin Surface Al2O3 Layers during Lithiation-Delithiation Cycles. *Nano Lett.* **2011**, *11*, 4188−4194.
(17) Karki, K.; Epstein, E.; Cho, J. H.; Jia, Z.; Li, T.; Picraux, S. T.; Wang, C. S.; Cumings, J. Lithium-Assisted Electrochemical Welding in Silicon Nanowire Battery Electrodes. *Nano Lett.* **2012**, *12*, 1392−1397.
(18) Liu, N.; Wu, H.; McDowell, M. T.; Yao, Y.; Wang, C. M.; Cui, Y. A Yolk-Shell Design for Stabilized and Scalable Li-Ion Battery Alloy Anodes. *Nano Lett.* **2012**, *12*, 3315−3321.
(19) Leung, K.; Qi, Y.; Zavadil, K. R.; Jung, Y. S.; Dillon, A. C.; Cavanagh, A. S.; Lee, S. H.; George, S. M. Using Atomic Layer Deposition to Hinder Solvent Decomposition in Lithium Ion Batteries: First-Principles Modeling and Experimental Studies. *J. Am. Chem. Soc.* **2011**, *133*, 14741−14754.
(20) Jung, Y. S.; Cavanagh, A. S.; Dillon, A. C.; Groner, M. D.; George, S. M.; Lee, S. H. Enhanced Stability of $LiCoO_2$ Cathodes in Lithium-Ion Batteries Using Surface Modification by Atomic Layer Deposition. *J. Electrochem. Soc.* **2010**, *157*, A75−A81.
(21) Jung, Y. S.; Lu, P.; Cavanagh, A. S.; Ban, C.; Kim, G. H.; Lee, S. H.; George, S. M.; Harris, S. J.; Dillon, A. C. Unexpected Improved Performance of ALD Coated LiCoO2/Graphite Li-Ion Batteries. *Adv. Energy Mater.* **2013**, *3*, 213−219.
(22) Piper, D. M.; Travis, J. J.; Young, M.; Son, S. B.; Kim, S. C.; Oh, K. H.; George, S. M.; Ban, C. M.; Lee, S. H. Reversible High-Capacity Si Nanocomposite Anodes for Lithium-ion Batteries Enabled by Molecular Layer Deposition. *Adv. Mater.* **2014**, *26*, 1596−1601.
(23) Dameron, A. A.; Seghete, D.; Burton, B. B.; Davidson, S. D.; Cavanagh, A. S.; Bertrand, J. A.; George, S. M. Molecular Layer Deposition of Alucone Polymer Films using Trimethylaluminum and Ethylene Glycol. *Chem. Mater.* **2008**, *20*, 3315−3326.
(24) Kresse, G.; Hafner, J. Ab-Initio Molecular-Dynamics Simulation of the Liquid-Metal Amorphous-Semiconductor Transition in Germanium. *Phys. Rev. B* **1994**, *49*, 14251−14269.
(25) Kresse, G.; Furthmuller, J. Efficient Iterative Schemes for Ab Initio Total-Energy Calculations using a Plane-Wave Basis Set. *Phys. Rev. B* **1996**, *54*, 11169−11186.
(26) Kresse, G.; Hafner, J. Ab-Initio Molecular-Dynamics for Open-Shell Transition-Metals. *Phys. Rev. B* **1993**, *48*, 13115−13118.
(27) Kresse, G. Ab Initio Molecular Dynamics Applied to the Dynamics of Liquid Metals and to the Metal-Non-Metal Transition. *J. Non-Cryst. Solids* **1996**, *207*, 833−840.
(28) Perdew, J. P.; Burke, K.; Ernzerhof, M. Generalized Gradient Approximation Made Simple. *Phys. Rev. Lett.* **1996**, *77*, 3865−3868.
(29) Blochl, P. E. Projector Augmented-Wave Method. *Phys. Rev. B* **1994**, *50*, 17953−17979.
(30) Kresse, G.; Joubert, D. From Ultrasoft Pseudopotentials to the Projector Augmented-Wave Method. *Phys. Rev. B* **1999**, *59*, 1758−1775.
(31) Becke, A. D. Density-Functional Thermochemistry. III. The Role of Exact Exchange. *J. Chem. Phys.* **1993**, *98*, 5648−5652.
(32) Perdew, J. P.; Wang, Y. Accurate and Simple Analytic Representation of the Electron-Gas Correlation Energy. *Phys. Rev. B* **1992**, *45*, 13244−13249.
(33) Wang, Y. X.; Nakamura, S.; Tasaki, K.; Balbuena, P. B. Theoretical Studies to Understand Surface Chemistry on Carbon Anodes for Lithium-Ion Batteries: How Does Vinylene Carbonate Play its Role as an Electrolyte Additive? *J. Am. Chem. Soc.* **2002**, *124*, 4408−4421.
(34) Wang, Y. X.; Nakamura, S.; Ue, M.; Balbuena, P. B. Theoretical Studies to Understand Surface Chemistry on Carbon Anodes for Lithium-Ion Batteries: Reduction Mechanisms of Ethylene Carbonate. *J. Am. Chem. Soc.* **2001**, *123*, 11708−11718.
(35) Ma, Y. G.; Balbuena, P. B. DFT Study of Reduction Mechanisms of Ethylene Carbonate and Fluoroethylene Carbonate on Li^+-Adsorbed Si Clusters. *J. Electrochem. Soc.* **2014**, *161*, E3097−E3109.
(36) Benitez, L.; Cristancho, D.; Seminario, J. M.; Martinez de la Hoz, J. M.; Balbuena, P. B. Electron Transfer through SEI Layers Formed on Si Anodes of Li-Ion Batteries. *Electrochim. Acta* **2014**, *140*, 250−257.
(37) Buttiker, M.; Imry, Y.; Landauer, R.; Pinhas, S. Generalized Many-Channel Conductance Formula with Application to Small Rings. *Phys. Rev. B* **1985**, *31*, 6207−6215.
(38) Landauer, R. Spatial Variation of Currents and Fields Due to Localized Scatterers in Metallic conduction. *IBM J. Res. Dev.* **1957**, *1*, 223−231.
(39) Landauer, R. Electrical Resistance of Disordered One-Dimensional Lattices. *Philos. Mag.* **1970**, *21*, 863−867.
(40) Landauer, R. Comment on Lodder Exact Electromigration Theory. *Solid State Commun.* **1989**, *72*, 867.
(41) Landauer, R. W. Irreversibility and Heat Generation in the Computing Process. *IBM J. Res. Dev.* **1961**, *5*, 183−191.
(42) Datta, S. *Electronic Transport in Mesoscopic Systems*; Cambridge University Press: Cambridge, U.K., 1995.
(43) Hall, R. A. Metalcone Chemistry: In Pursuit of Improved Mechanical Properties in Thin Film Deposition. Ph.D. Dissertation, University of Colorado at Boulder, July 2013.
(44) Shi, S. Q.; Lu, P.; Liu, Z. Y.; Qi, Y.; Hector, L. G.; Li, H.; Harris, S. J. Direct Calculation of Li-Ion Transport in the Solid Electrolyte Interphase. *J. Am. Chem. Soc.* **2012**, *134*, 15476−15487.
(45) Kim, S. Y.; Qi, Y. Property Evolution of Al_2O_3 Coated and Uncoated Si Electrodes: A First Principles Investigation. *J. Electrochem. Soc.* **2014**, *161*, F3137−F3143.
(46) Martinez de la Hoz, J. M.; Balbuena, P. B. Reduction Mechanisms of Additives on Si Anodes of Li-Ion Batteries. *Phys. Chem. Chem. Phys.* **2014**, *16*, 17091−8.
(47) Martinez de la Hoz, J. M.; Leung, K.; Balbuena, P. B. Reduction Mechanisms of Ethylene Carbonate on Si Anodes: Effects of Degree of Lithiation and Nature of Exposed Surface. *ACS Appl. Mater. Interfaces* **2013**, *5*, 13457−13465.
(48) Leung, K.; Rempe, S. B.; Foster, M. E.; Ma, Y.; Martinez-delaHoz, J. M.; Sai, N.; Balbuena, P. B. Modeling Electrochemical Decomposition of Fluoroethylene Carbonate on Silicon Anode Surfaces in Lithium Ion Batteries. *J. Electrochem. Soc.* **2014**, *3*, A213−221.

DOI: 10.1021/acsami.5b01917
ACS Appl. Mater. Interfaces 2015, 7, 11948−11955